ADVANCED FUNCTIONAL MATERIALS
www.afm-journal.de

Transferred Chiroptical Transitions in Chiral Binaphthyl /π-Conjugated Polymer Hybrid Films: Significance of Aromatic Solvent-Mediated Co-Crystallization

*Hanna Lee, Wassie M. Takele, Jong Ik Kwon, Changsoon Choi, Danbi Kim, Jeong Ho Cho, Terefe G. Habteyes, and Jung Ah Lim**

For advancing next-generation optoelectronics, a versatile strategy for fabricating π-conjugated polymer (π-CP)/*chiral*-small molecule (SM) hybrid films through co-crystallization-mediated chirality transfer is reported. The transfer of optical chirality from 1,1′-binaphthyl–2,2′-diamine (BN), a representative chiral inducer SM, to thin films of various achiral π-CPs, including non-fluorene π-CPs, is achieved by simply blending the π-CPs with BN using aromatic organic solvents. The resulting π-CP/*chiral*-SM hybrid films exhibit chiroptical responses at the main electronic absorption bands of various π-CPs. Studies of the morphology, crystalline structure, and phase-separation structure of a representative hybrid system of poly(3-hexylthiophene) (P3HT) and BN reveal that these hybrid films exhibit a characteristic lamellar structure where the π-CPs co-crystallize with chiral BN molecules, facilitated by aromatic solvent-assisted intermolecular π–π interactions. In-depth photophysical analysis suggests that BN molecules co-crystallized in the P3HT lamellar structure induce asymmetrically misaligned transition dipoles along the P3HT conjugated backbone, transferring optical chirality from BN to P3HT under circularly polarized light illumination. As a proof-of-concept, chiroptical photodiodes based on π-CP/*chiral*-SM hybrid films and printed micropatterns, exhibiting a distinguishable photocurrent response depending on the direction of circularly polarized light are successfully demonstrated.

1. Introduction

The development of chiral optoelectronic materials capable of interacting with circularly polarized light (CPL) has gained significant attention as a key technology for propelling next-generation optoelectronic technologies. In particular, anisotropic opto-magnetic interactions of semiconducting materials with CPL enable optoelectronic devices to control the electron's nature of charges, light, and spin, opening up new possibilities in opto-magnetic, spin, and quantum-based electronics for various applications, such as quantum computing, spintronics, cryptography, 3D and bio-imaging, displays, and pharmaceuticals.[1–6] Recent advances in solution-processable chiral nanomaterials, such as metal or inorganic nanoparticles,[7] small conjugated molecules,[8–10] conjugated polymers,[11,12] and halide perovskites,[13,14] facilitate the easy fabrication of chiral optoelectronic devices. This approach has become highly promising to overcome the current limitations of miniaturization and

H. Lee, D. Kim, J. A. Lim
Soft Hybrid Materials Research Center
Korea Institute of Science and Technology
Seoul 02792, Republic of Korea
E-mail: jalim@kist.re.kr

H. Lee, D. Kim, J. H. Cho
Department of Chemical and Biomolecular Engineering
Yonsei University
Seoul 03722, Republic of Korea

W. M. Takele, T. G. Habteyes
Department of Chemistry and Chemical Biology
University of New Mexico
Albuquerque, NM 87131, USA

J. I. Kwon, C. Choi
Center for Opto-Electronic Materials and Devices
Korea Institute of Science and Technology
Seoul 02792, Republic of Korea

J. I. Kwon
Department of Materials Science and Engineering
Ulsan National Institute of Science and Technology
Ulsan 44919, Republic of Korea

J. A. Lim
Division of Nanoscience and Technology
KIST School
University of Science and Technology (UST)
Seoul 02792, Republic of Korea

J. A. Lim
Department of Materials Science and Engineering
YU-KIST Institute
Yonsei University
Seoul 03722, Republic of Korea

The ORCID identification number(s) for the author(s) of this article can be found under https://doi.org/10.1002/adfm.202409982

DOI: 10.1002/adfm.202409982

integration by bulky optical components, such as linear polarizers and quarter-wave plates, which are commonly used to generate or respond to CPL.[15,16]

Among the various chiroptical nanomaterials, chiral π-conjugated polymers (*chiral* π-CPs) have emerged as a leading advancement in the field of organic electronics owing to their characteristics, including ease of uniform thin-film formation, excellent optical and electrical properties, and compatibility with flexible, large-area-device architectures, making them a compelling choice to extend the era of future chiral optoelectronics.[17,18] To impart chiroptical activity to π-CPs, induction of the rotated charge displacement in the π-CP in the photoexcitation state is required. One of the important features of *chiral* π-CPs is that their chiroptical response can be transferred or amplified through exciton coupling in the dissymmetrical or twisted stacking of π-conjugation building blocks.[19,20] To date, three primary approaches have been primarily explored to implement *chiral* π-CPs: i) The first basic approach involves incorporating chiral functional groups into the conjugated backbone or side chains of π-CPs.[17,21] This approach manifests the chiroptical response of π-CPs. However, optimizing the synthesis of the desired molecular structure and the optoelectronic properties of their thin-film structures for the realization of high-performance chiroptical devices requires considerable effort. ii) As a simple approach, the use of chiral organic solvents, such as (*R* or *S*)-limonene[22,23] and (1*R* or 1*S*)-α-pinenes,[24,25] has been demonstrated to generate chiroptical absorption in achiral π-CP aggregates. It has been reported that liquid crystalline polymers, such as poly[(9,9-dioctylfluorenyl-2,7-diyl)-*co*-bithiophene] (F8T2), or polymers derived from acetylene with aromatic pendants, exhibit more effective chirality. However, chirality induction from such chiral solvents is not universally effective for various π-CPs. iii) As a promising alternative strategy, π-CPs hybrid with chiral small molecule (π-CP/*chiral*-SM hybrid) have attracted significant research interest.[26–28] This approach enables the integration of numerous achiral π-CPs with diverse optical and electrical properties and the strong chiral activity of naturally occurring or readily accessible small molecules. Previous literature has demonstrated the successful creation of π-CP/*chiral*-SM hybrid thin films based on various achiral π-CPs, including polythiophenes, polyfluorenes, acetylene-derived polymers, and benzodithiophenedione-based polymers, by blending them with various chiral small molecules, such as binaphthyl derivatives, helicene derivatives, and amino acids.[29–31] Recent advancements in CPL-sensing photodetectors[26,32–34] and circularly polarized organic light-emitting diodes[35–38] utilizing π-CP/*chiral-SM* hybrid thin films have highlighted the potential of these materials for chiral optoelectronic devices. Despite the importance of research on *chiral* π-CP hybrid materials for the development of chiral optoelectronic devices, a fundamental understanding of how the chirality of small molecules can be transferred to achiral π-CPs in π-CP/*chiral*-SM hybrid systems has not yet been fully elucidated.

In previous research on supramolecular self-assembly studies, there have been extensive demonstrations regarding the transfer of chirality from the helical building blocks of chiral molecules to achiral π-conjugated molecules.[39] It is evident that the co-assembly of π-conjugated molecules via diverse non-covalent interactions, including interamide interactions,[40] cooperative hydrogen bonds,[41] chain interdigitation,[42] or π–π stacking interactions[43] can induce the twisted or helical assembly of π-conjugated cores, leading to new chiroptical electronic transitions in achiral π-conjugated molecules. However, compared to supramolecular chirality transfer, studies on the molecular-level origin of chiroptical responses from achiral π-CPs in π-CP/*chiral*-SM hybrids have been rarely reported. The morphologies or crystalline structures of π-CP/*chiral*-SM hybrid films do not resemble mesoscopic helixes or twisted structures, making it challenging to elucidate whether the chirality induction in π-CP/*chiral*-SM hybrid films originates from the structural twist assembly of the π-CP backbone. Recently, Wade et al. proved through comparison with the simulation of optical activity that the strong chiroptical responses of π-CP/*chiral*-SM hybrids based on the blend of polyfluorenes and helicene chiral additives may stem from in-plane helical modulation of polymer fibrils in a double twist cylinder-type blue phase.[30] Recently, Song et al. demonstrated that blends of the binaphthyl chiral molecules with the π-CP incorporating fluorene moiety formed supramolecular helices of π-CP, leading to columns with their long axis aligned in the in-plane direction.[26] In this study, binaphthyl chiral molecules served as templates for helical stacks of polymer chains rather than forming complexes with the polymer chains. Consequently, the strong chiroptical response of the hybrid film was retained after the removal of binaphthyl chiral dopants through thermal annealing. However, previous studies have primarily focused on hybrids of polyfluorenes, and the mechanism by which chiral molecules induce helical stacks of π-CP remains unclear. Furthermore, no versatile strategies for inducing chiroptical responses in non-fluorene π-CPs via hybrids of chiral small molecules have been proposed thus far.

In this regard, although poly(3-alkylthiophene) (P3AT) is one of the most well-known and intensively studied π-CP semiconductors for various organic electronic devices, chiroptical electronic transitions in P3AT thin films through simple blending with chiral additives have rarely been reported. The chiroptical activity of polythiophenes has been achieved by substituting alkyl sidechains with enantiopure moieties[44,45] or carboxylated alkyl sidechains for suspension blending with chiral cellulose nanocrystals, as reported previously.[46] For example, a blend of achiral carboxylic acid functionalized poly(3-alkylthiophene) (P3CT) and chiral binaphthyl molecules was used to fabricate chiroptical polythiophene thin films.[47] The chiroptical response of binaphthyl molecules was amplified by forming a vertically phase-separated bilayer structure; however, the optical chirality of binaphthyl molecules was not transferred to P3CT, as evidenced by the absence of chiroptical response at the main absorption band of P3CT.

In this study, we proposed a versatile strategy for fabricating π-CP/*chiral*-SM hybrid films based on co-crystallization-mediated chirality transfer using 1,1′-binaphthyl-2,2’-diamine (BN), a representative chiral small molecule. Chiral binaphthyl derivatives are well-known enantiomers used in various applications that exhibit a preference for highly rigid planar conformations based on the anchored dihedral angle of their binaphthyl group.[48–51] This structural characteristic facilitates the amplification of intrinsic molecular chirality and enhances their chirality induction ability.[37,52,53] A key finding of this work is that the π-CP/*chiral*-BN hybrid films exhibit chiroptical responses at each primary electronic absorption band of various achiral π-CPs when simply

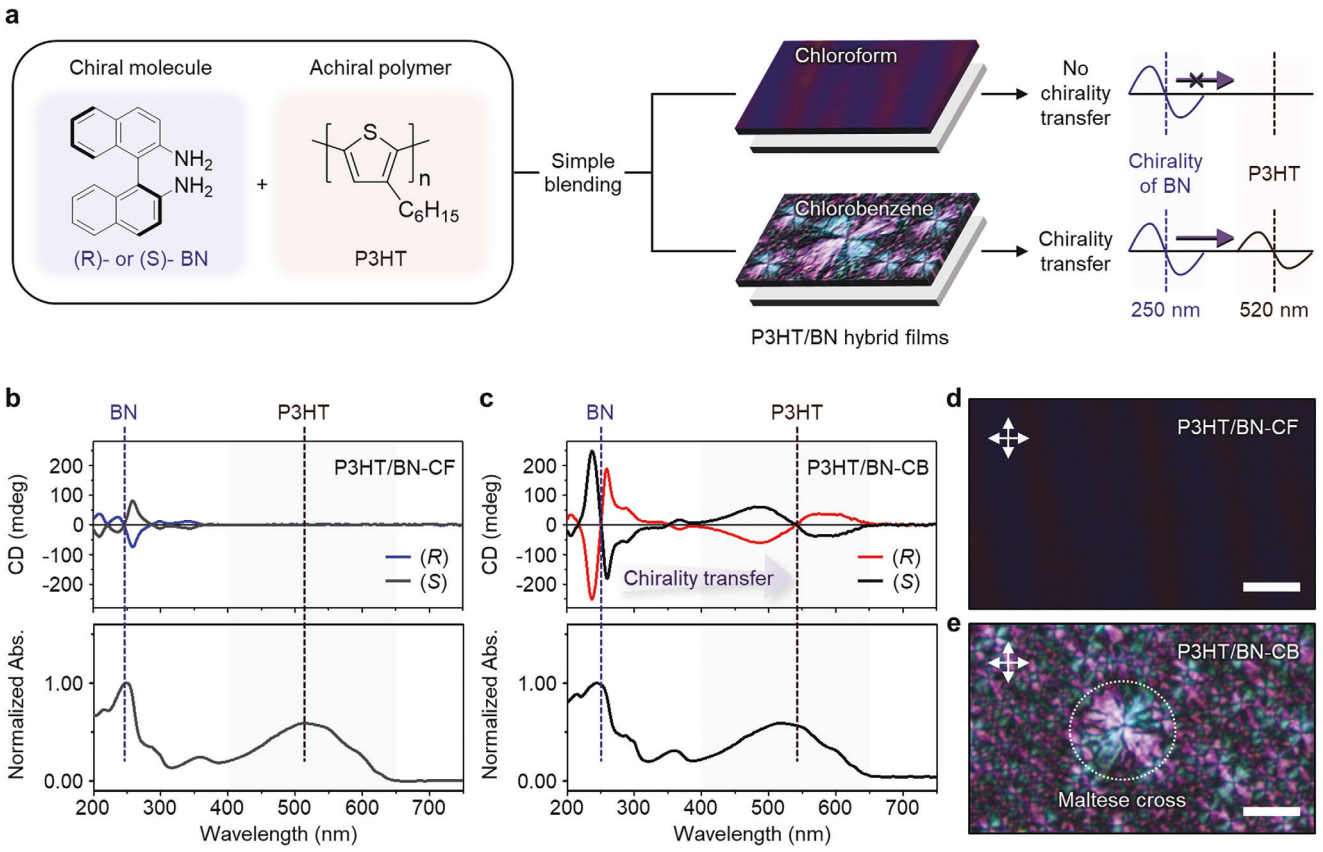

Figure 1. a) Chemical structures of a chiral molecule (1,1′-binaphthyl–2,2′-diamine (BN)) and achiral π-conjugated polymer (poly(3-hexylthiophene) (P3HT)) and a schematic illustration of the fabrication of P3HT/BN hybrid film using chloroform (CF) or chlorobenzene (CB). Solvent-dependent chirality transfer in the P3HT/BN hybrid was observed. b,c) Circular dichroism (CD) spectra (top) and normalized optical absorption (bottom) of P3HT/BN hybrid film using CF (P3HT/BN-CF, b)) and CB (P3HT/BN-CB, c)). The shaded area is the primary absorption band of P3HT. d–e) Polarized optical microscopy (POM) images of P3HT/BN-CF (d) and P3HT/BN-CB (e) films (polarization angle = 90°, scale bar = 20 µm).

blending the π-CPs with BN especially using aromatic organic solvents. Studies on the morphologies, crystalline, and phase-separation structure of a representative hybrid system of poly(3-hexylthiophene) (P3HT) and BN, revealed that these π-CP/*chiral*-SM hybrid films have a characteristic lamellar structure where the π-CPs are co-crystallized with chiral BN molecules by aromatic solvent-assisted intermolecular π–π interactions. Based on the photophysical analysis, we found that π–π interactions of aromatic CB molecule with P3HT might hinder the formation of P3HT aggregation, enhancing co-crystallization of BN and P3HT backbone. The result suggested that the adjacent BN molecules interacting with the P3HT chain induce the asymmetric misaligned transition dipoles along the P3HT backbone, resulting in the transfer of optical chirality from BN to P3HT. The chiroptical photodiodes based on π-CP/*chiral*-SM hybrid films were demonstrated, showing a distinguishable photocurrent difference according to the circular polarization direction of the incident light.

2. Results and Discussion

Figure 1a shows a schematic of the preparation of chiroptical BN and P3HT hybrid films, referred to as P3HT/BN hybrid films, which have been studied as representative model systems for π-CP/*chiral*-SM hybrid films. Figure 1b,c show the circular dichroism (CD) spectra of P3HT/BN hybrid films spin-cast from a blended solution with two different chlorinated solvents, chloroform (CF) and chlorobenzene (CB), both of which tend to dissolve the P3HT and BN molecules. The P3HT/BN hybrid film prepared using the CF solution (P3HT/BN-CF) exhibited a CD response only from the BN additives in the absorption range of 200–360 nm. In contrast, the P3HT/BN film coated with the CB solution (P3HT/BN-CB) exhibited a mirror-imaged signal corresponding to the chirality of BN in the 200–650 nm absorption band with a strong Cotton effect at 540 nm, corresponding to the main optical transitions in P3HT (shaded area). This spectroscopic evidence confirmed chirality transfer from BN to achiral P3HT, wherein the photoexcited state of P3HT splits into two exciton levels induced by hybridization with chiral BN. An increase in the chirality-transferred CD response of the P3HT/BN-CB films with higher BN contents is observed, as shown in Figure S1 (Supporting Information). The maximum BN content in this hybrid was limited to 33 wt.%, owing to the incomplete dissolution of BN, which led to precipitation when the BN content exceeded this threshold. The absorption dissymmetry factor (g_{abs}) of P3HT/BN-CB film is $\approx 3.8 \times 10^{-3}$ at 473 nm (Figure S1a, Supporting Information), which falls within the typical range of 10^{-4} to 10^{-0} observed in previously reported chiroptical π-CP thin films.[54–57] We confirmed that this chiroptical response was not

attributed to macroscopic anisotropies, such as birefringence or linear dichroism. Negligible differences are observed in the CD spectra when the films are viewed from the front and back or when the azimuthal angle of the sample is rotated around the optical axis of the incident light (Figure S2, Supporting Information).

Notably, this solvent-dependent chirality transfer in the P3HT/BN hybrid was only observed in the solid film. The CD spectra of the blended solutions are identical to those of the BN-only solutions (Figure S3, Supporting Information). The CD couplet of 1,1′-binaphthyl derivatives is dependent on the torsion angle of the dihedral link, influencing the electronic transitions and coupling between the π and π^* transitions of the molecule.[58–60] This finding implies that the rotational charge displacement in the photoexcited BN molecules did not change after blending with P3HT in a well-dissolved solvent. However, different from the CD response of the P3HT/BN-CF film, which is nearly identical to that in its solution state, a different coupling signal for BN was observed for the P3HT/BN-CB hybrid film. This result indicates that the transition dipoles of BN molecules definitely changed only when the P3HT/BN hybrid film was fabricated using CB solvent. The rotational transition dipole moments were newly generated in the photoexcited P3HT phase by intermolecular interactions with BN.

Figure 1d,e shows the cross-polarized optical microscopy (POM) images of the P3HT/BN-CF and P3HT/BN-CB films, respectively. In contrast to the P3HT/BN-CF film, which did not exhibit any response under cross-polarized light, the P3HT/BN-CB film exhibited a characteristic extinction pattern with a 4-fold symmetry, known as the Maltese cross pattern. This finding indicates the formation of polymer spherulites with optically anisotropic crystalline lamellar structures,[61–63] particularly in P3HT/BN-CB films, which exhibit chiroptical transitions induced in P3HT. Because the P3HT-pristine films spin-cast from the CB solution usually did not show such spherulitic-birefringence, we can rationalize that the hybrid with BN in the CB solvent resulted in lamellar crystallization of P3HT during the spin-coating process. Notably, this solvent-dependent chirality transfer and spherulite structure development were also observed in blade-coated films, indicating that it is not an effect of the spin-casting process (Figure S4, Supporting Information). We found that these morphologies extend throughout the entire film thickness, as demonstrated by the POM images of both the front and back sides of P3HT/BN-CB coated on quartz (Figure S5, Supporting Information). In addition, the POM images of P3HT/BN-CB did not exhibit 2D-ring banded periodic extinction patterns, indicating the absence of twisted lamellar alignment.[62] Instead, it can be explained that continuous radial packing of P3HT lamellar with varied orientations was formed in the P3HT/BN-CB hybrid film.[64] Moreover, the formation of these spherulitic patterns, based on the lamellar organization of polymers, is also known to be influenced by film-forming conditions such as the solvent evaporation rate.[65] To verify the effect of fast evaporation of CF (61 °C) compared to that of CB (132 °C), further morphological development in P3HT/BN-CF hybrid films is examined using slow drop-casting in a closed jar (Figure S6, Supporting Information). Consequently, no spherulite structures are observed in the P3HT/BN-CF hybrid film, in which a weaker CD response (more than 10 times) is observed at the absorption transition of P3HT. This finding implies that slow evaporation of the CB solvent may not be the primary cause of spherulitic crystallization in the P3HT/BN hybrid. In contrast, the aromatic solvent CB plays a critical role in inducing lamellar crystallization of P3HT and BN, contributing to the chiroptical activity of the hybrid films.

To emphasize the significance of the aromatic solvents, various aromatic solvents, including toluene, *o*-xylene (xylene), 1,2-dichlorobenzene (DCB), tetrahydronaphthalene (tetralin), and 1,2,4-trichlorobenzene (TCB), are tested for the P3HT/BN hybrid films. **Figure 2a–h** shows the chiroptical response and POM images of the P3HT/BN hybrid films cast using various aromatic solvents with different boiling points. Notably, all films exhibited a distinct chiroptical response at the optical transition of P3HT with Maltese cross spherulites in the POM images. The demonstrated (*R*)-P3HT/BN hybrid films using the (*R*)-enantiomer BN, cast from different aromatic solvents, exhibited a negative Cotton effect at 540 nm, corresponding to the main optical transition of P3HT, identical to the previously mentioned (*R*)-P3HT/BN-CB hybrid film. This consistency implies that the transition dipoles generated in the chirality-transferred P3HT of the P3HT/BN hybrid films were similar regardless of the aromatic solvent used. These observations verified that aromatic solvents are crucial in inducing chirality transfer from chiral molecules to achiral π-CP and spherulitic crystallization in π-CP/*chiral*-BN hybrids. Moreover, using TCB with a high boiling point (214 °C), arrays of micropatterns were successfully printed using a direct-writing fluidic dispenser. Figure 2i exhibits circular micropattern arrays with a diameter of 240 µm, where one spherulite domain expanded from a single nucleus center is formed. To our knowledge, this is the first demonstration of a chiroptically printed micropattern of π-CPs films.

To explore the broad applicability of this chirality transfer strategy, hybrids with chiral BN are fabricated using various achiral π-CPs, which have been extensively studied for use in organic optoelectronic devices (**Figure 3a**). These polymers include poly(9,9-di-*n*-octylfluorenyl-2,7-diyl) (PFO),[66] which is a light-emitting material for high-efficiency OLED devices, and poly[[4,8-bis[(2-ethylhexyl)oxy]benzo[1,2-*b*:4,5-b′]dithiophene-2,6-diyl][3-fluoro-2-[(2-ethylhexyl)carbonyl]thieno[3,4-*b*]thiophenediyl]] (PTB7),[67] recognized for donor-acceptor type semiconductor polymer with superior light absorption properties in organic photovoltaics, and poly[(2,5-bis-(2-octyldodecyl)−3,6-bis-(thien-2-yl)-pyrrolo[3,4-*c*]pyrrole-1,4-diyl)-*co*-(2,2′-(2,1,3-benzothiadiazole)]−5,5′-diyl)] (P(DPPTBT)),[68] characterized by a diketopyrrolopyrrole-based copolymer exhibiting a low bandgap and high mobility. Figure 2b–d shows the CD spectra of the PFO/BN, PTB7/BN, and P(DPPTBT)/BN hybrid films prepared using the aromatic solvent toluene. All hybrid films prepared using toluene exhibited distinct chirality-transferred optical transitions, exhibiting designated CD signals at each primary absorption band (shaded area) of the π-CPs. Interestingly, these chiroptical hybrid films based on various π-CPs exhibit Maltese-cross spherulite morphologies, as shown in Figure 3e–g of the POM images. Conversely, when the CF solvent is used, no chirality transfer occurs to the π-CPs and Maltese-cross spherulite (Figure S7, Supporting Information). This solvent-dependent chirality transfer and crystallization behavior were consistent with the findings in the P3HT/BN hybrid films, as described above. Furthermore,

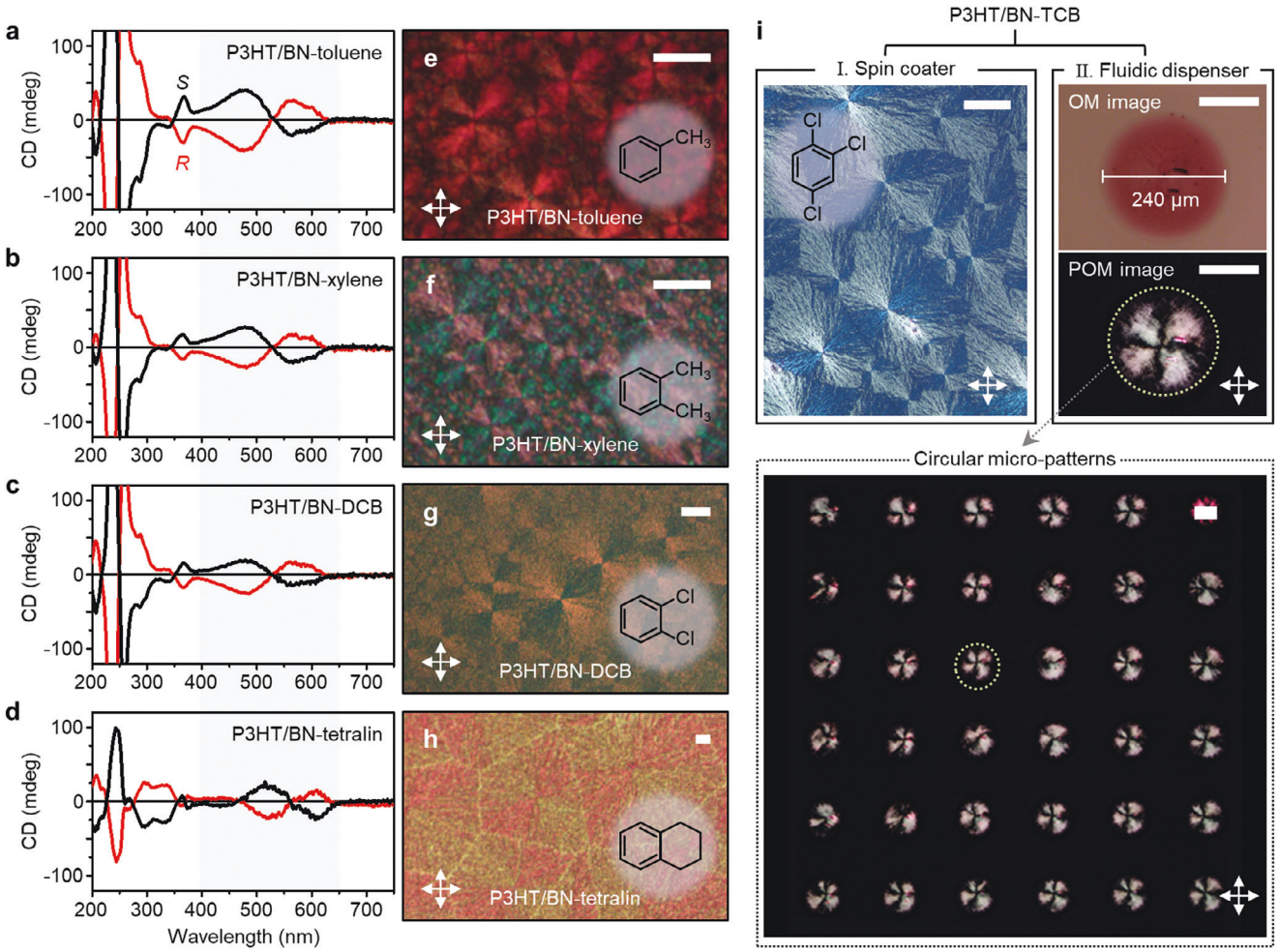

Figure 2. a–d) CD spectra of P3HT/BN hybrid films using toluene (P3HT/BN-toluene, (a)), *o*-xylene (P3HT/BN-xylene, (b)), 1,2-dichlorobenzene (P3HT/BN-DCB, (c)) and tetrahydronaphthalene ((P3HT/BN-tetralin, (d)) fabricated using spin-casting method. e–h) POM images of P3HT/BN-toluene (e), P3HT/BN-xylene (f), P3HT/BN-DCB (g) and P3HT/BN-tetralin (h) (polarization angle = 90°, scale bar = 20 μm). i) POM image of P3HT/BN hybrid films fabricated using spin-casting method (I). OM (top of II) and POM image (bottom of II) of P3HT/BN printed droplets using a direct-writing fluidic dispenser (II), which obtains 240 μm circular micro-patterns. 1,2,4-trichlorobenzene (TCB) with a high boiling point (214 °C) is used as a solvent (polarization angle = 90°, scale bar = 100 μm).

the circular micropattern printing was also successfully achieved with P(DPPTBT)/BN hybrid using TCB solvent, as shown in Figure S8 (Supporting Information). This result indicates that the π-CP/*chial*-SM hybrid strategy can be applied to achieve chiroptical activity in a diverse range of π-CP materials. Furthermore, spherulitic crystallization is essential to transferring the chiroptical activity of achiral π-CPs in the hybrid films, which can be significantly affected by the use of aromatic solvents in the solution hybrid process.

To gain a comprehensive understanding of the formation of spherulite structure and the resulting chiroptical response in π-CP/*chiral*-BN hybrid films, we specifically conducted focused research on P3HT/BN hybrid films. First, the surface morphologies of the P3HT/BN hybrid films were analyzed using atomic force microscopy (AFM). As shown in **Figure** 4a–c, the P3HT/BN-CF film exhibits a featureless, smooth surface (root-mean-square surface roughness of 1.3 nm), whereas the P3HT/BN-CB film shows a spherulite structure comprising interconnected nanogranules that radially extend from the nuclei center. The size of the nanogranules was ≈360–450 nm, as observed in the scanning electron microscopy image (Figure S9, Supporting Information). The magnified image shown in Figure 4c reveals that this nanogranule is an aggregate of a layered lamellar with a step height of ≈1.8 nm, consistent with the well-known interlamellar distance of P3HT stacking.[69] To elucidate the chemical composition inside the nanogranules of the P3HT/BN hybrid film, we visualized localized BN using scattering-type scanning near-field optical microscopy (s-SNOM).[70] As shown in the Fourier transform infrared (FT-IR) spectra (Figure S10, Supporting Information), the absorption at 1616 cm^{-1}, corresponding to the N–H stretching vibration, was observed only in BN. Therefore, a higher phase shift can be observed when the metalized AFM probe interacts with the BN component at an excitation frequency of 1616 cm^{-1}, resulting in the visualization of the BN-rich phase (red) and P3HT-rich phase (blue) in phase images ((*ii*) of Figure 4d,e). The specific interaction-driven phase

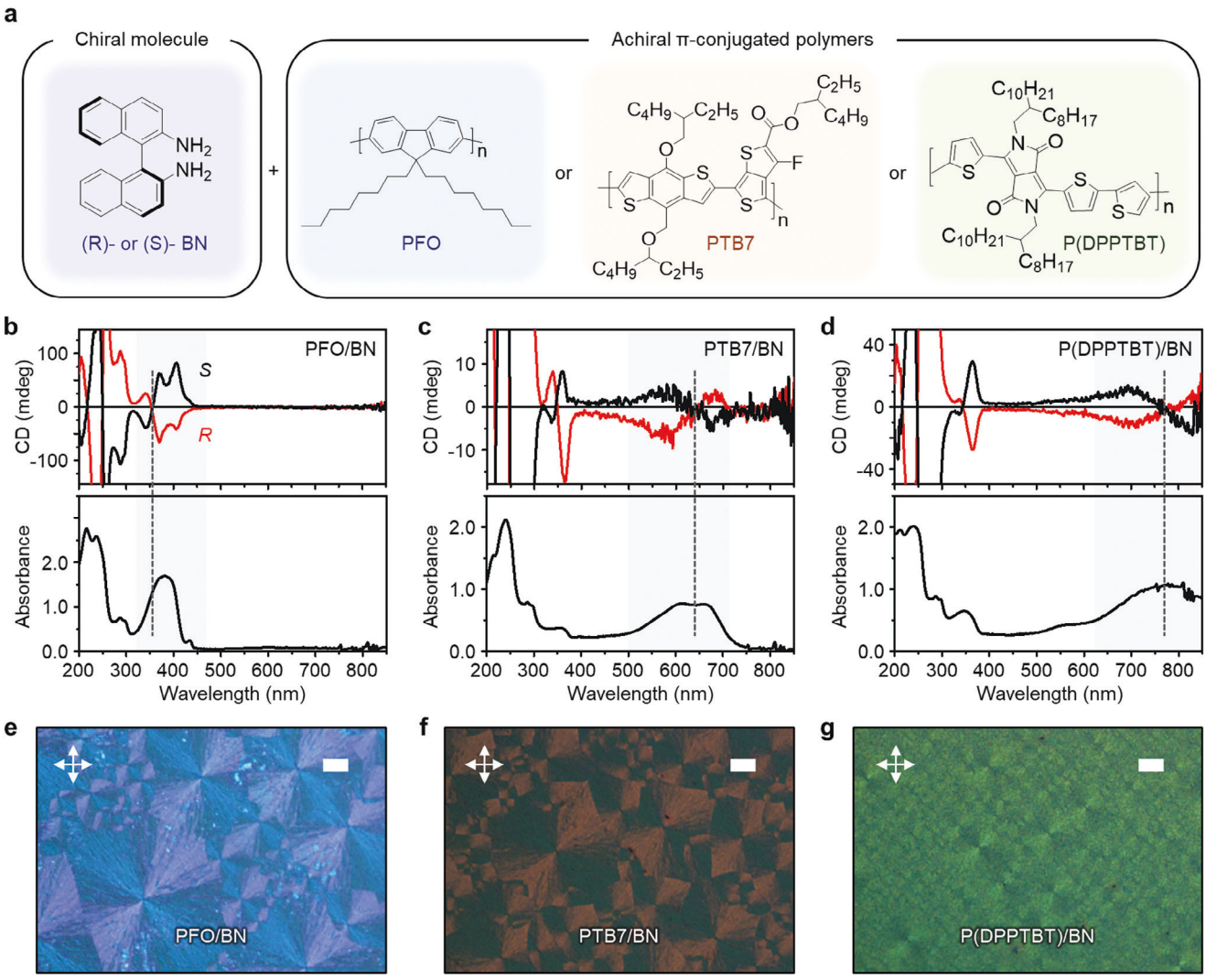

Figure 3. a) Chemical structures of the chiral molecule (BN) and achiral π-conjugated polymers (poly(9,9-di-*n*-octylfluorenyl-2,7-diyl) (PFO), poly[[4,8-bis[(2-ethylhexyl)oxy]benzo[1,2-*b*:4,5-b']dithiophene-2,6-diyl][3-fluoro-2-[(2-ethylhexyl)carbonyl]thieno[3,4-*b*]thiophenediyl]] (PTB7), and poly[(2,5-bis-(2-octyldodecyl)−3,6-bis-(thien-2-yl)-pyrrolo[3,4-*c*]pyrrole-1,4-diyl)-*co*-(2,2′-(2,1,3-benzothiadiazole)]−5,5′-diyl)] (P(DPPTBT))) b–d) CD spectra (top) and optical absorption (bottom) of hybrid films fabricated by simply blending the achiral π-conjugated polymers with BN using an aromatic organic solvent of toluene. PFO (PFO/BN, (b)), PTB7 (PTB7/BN, (c)), and P(DPPTBT) (P(DPPTBT)/BN, (d)) are used as achiral π-conjugated polymers. The shaded area is the primary absorption band of achiral π-conjugated polymers. e–g) POM images of PFO/BN (e), PTB7/BN (f), and P(DPPTBT)/BN (g) hybrid films prepared using aromatic solvent, toluene (polarization angle = 90°, scale bar = 20 µm).

shift is verified by comparing different near-field images at an off-resonance frequency of 1540 cm^{-1} ((*iii*) in Figure 4d,e). For the P3HT/BN-CF film, as shown in Figure 4d, the BN molecules are uniformly distributed on the smooth film surface. In contrast, the BN molecules are concentrated at the nanogranules of the P3HT/BN-CB film, as shown in Figure 4e. This result verifies that the P3HT and BN co-crystallize into nanogranules when the CB is used in the film-forming process.

To understand the co-crystallization behaviors of the P3HT/BN hybrids, the thermal transitions of the films were analyzed using differential scanning calorimetry (DSC). **Figure 5** shows the DSC thermograms of pristine P3HT, BN, P3HT/BN-CF, and P3HT/BN-CB, collected from the casted films. P3HT and BN exhibited single melting transitions (T_m) at 228 and 244 °C, respectively. Notably, a new endothermic transition at 215 °C was observed for both P3HT/BN-CF and P3HT/BN-CB, which was lower than the T_m of P3HT and BN. This finding signifies strong evidence for the presence of a newly generated co-crystalline phase of P3HT and BN in the hybrid film. In contrast to the pristine P3HT and BN, new exothermic cold crystallization transitions (T_{cc}) were distinctly observed at 90 °C only for P3HT/BN-CF. Cold crystallization indicates the presence of amorphous chains in the quenched state that can readily crystallize at temperatures slightly above the glass transition temperature.[71] This finding suggests that the presence of BN in the hybrid can enhance the crystallization of P3HT, whereas the amorphous P3HT chains that do not participate in crystallization remain when the hybrid film is prepared using a CF solvent. In contrast, the

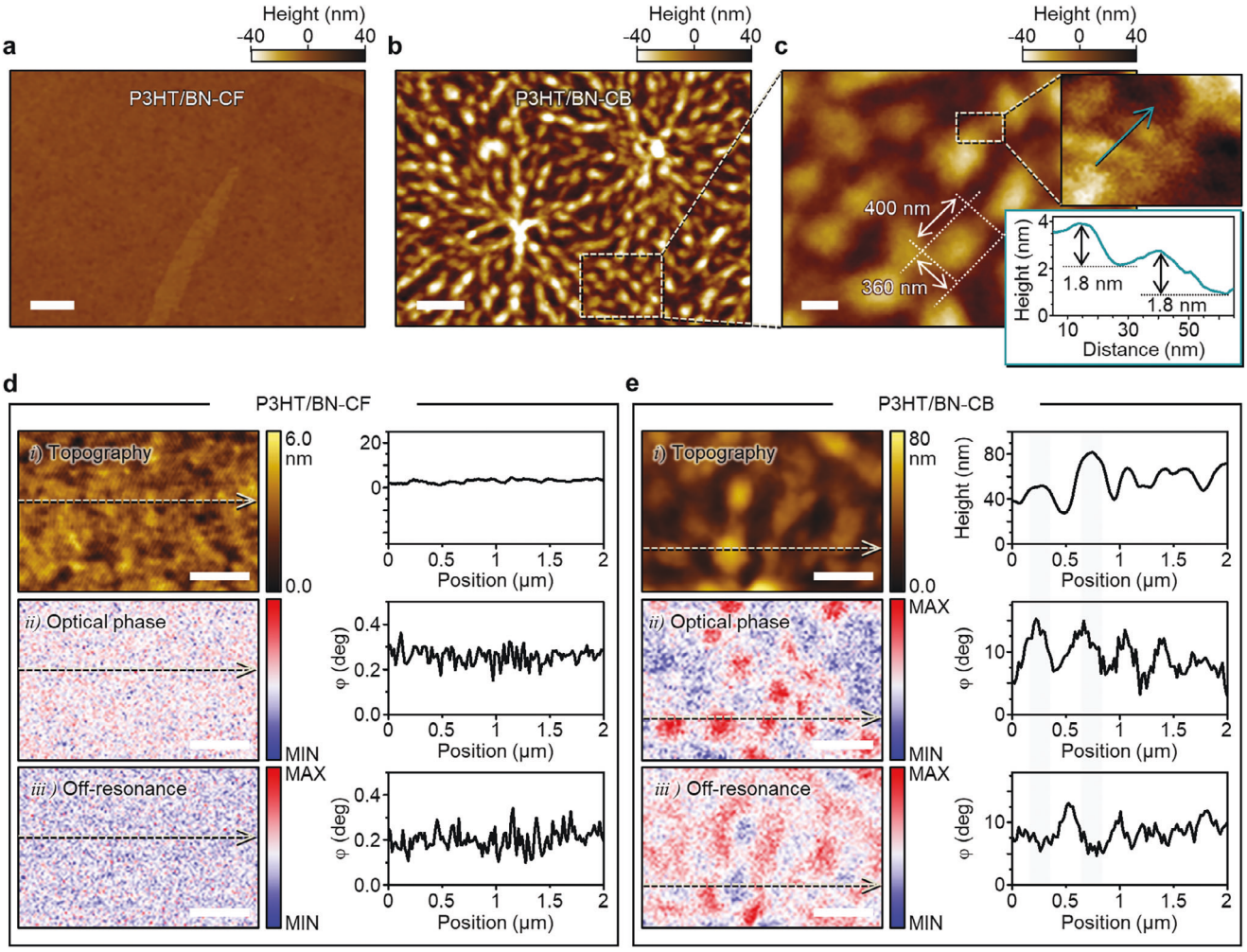

Figure 4. a–b) Atomic force microscopy (AFM) images of P3HT/BN-CF (a) and P3HT/BN-CB (b) hybrid films (scale bar = 1 μm). c) Magnified AFM images in (b) (scale bar = 200 nm). Insets show its magnified image (top) and height profile obtained from arrows marked in green (bottom). d–e) Small area scan showing AFM topography i) and IR near-field phase images measured using IR light at an on-resonance frequency of 1616 cm^{-1} ii) and an off-resonance frequency of 1540 cm^{-1} iii) of P3HT/BN-CF (d) and P3HT/BN-CB (e). Line profile of the corresponding topography and IR near-field phase at 1616 and 1540 cm^{-1} obtained from arrows marked in beige.

absence of T_{cc} in P3HT/BN-CB indicated the formation of crystallites in the P3HT/BN-CB film, with a significantly reduced amorphous phase compared to that of the P3HT/BN-CF film. The second main endothermic transition at 239 °C observed in the subsequent heating process was attributed to the sublimation of the segregated BN phase in the hybrid. This finding is supported by the disappearance of the CD response and absorption peak of the BN when the P3HT/BN-CB film is thermally annealed at 160 °C for 10 min (Figure S11, Supporting Information). In contrast to P3HT/BN-CB, P3HT/BN-CF exhibited an endothermic hump at 222 °C, which was attributed to the phase-separated P3HT. This phase separation is further supported by the two distinct crystallization transitions observed at 171 and 161 °C during the cooling process (see Figure 5b). For P3HT/BN-CB, no endothermic hump was observed, and a single crystallization transition was observed at 169 °C during the cooling process, indicating that the co-crystal was formed without phase separation. Based on these results, we can conclude that the aromatic CB solvent results in thermodynamically favorable co-crystallization of BN and P3HT in the hybrid films, whereas phase separation can occur in the hybrid film prepared from the CF solvent.

The co-crystalline structure and molecular orientation of the P3HT/BN hybrid films were investigated using grazing incident X-ray diffraction (GIXD) analysis. **Figure 6**a,b illustrate the unit cell structures of P3HT and BN crystals, respectively.[72,73] The 2D GIXD results of the P3HT-CF and P3HT/BN-CF films, as shown in Figure 6c,f, exhibit (010) and (100) diffraction in the out-of-plane (vertical direction, q_z) and in-plane (horizontal direction, q_{xy}) directions, respectively. This finding indicates that P3HT maintained a face-on orientation without any change in orientation after BN hybridization. The 1D plot results also confirmed that there are no evident changes in the d-spacing of the P3HT crystalline structure owing to BN hybridization (Figure 6i,k). In contrast, P3HT/BN-CB exhibits distinctive (l00) and (010) diffractions along the out-of-plane (q_z) and in-plane (q_{xy}) directions, respectively, similar to the P3HT film cast using

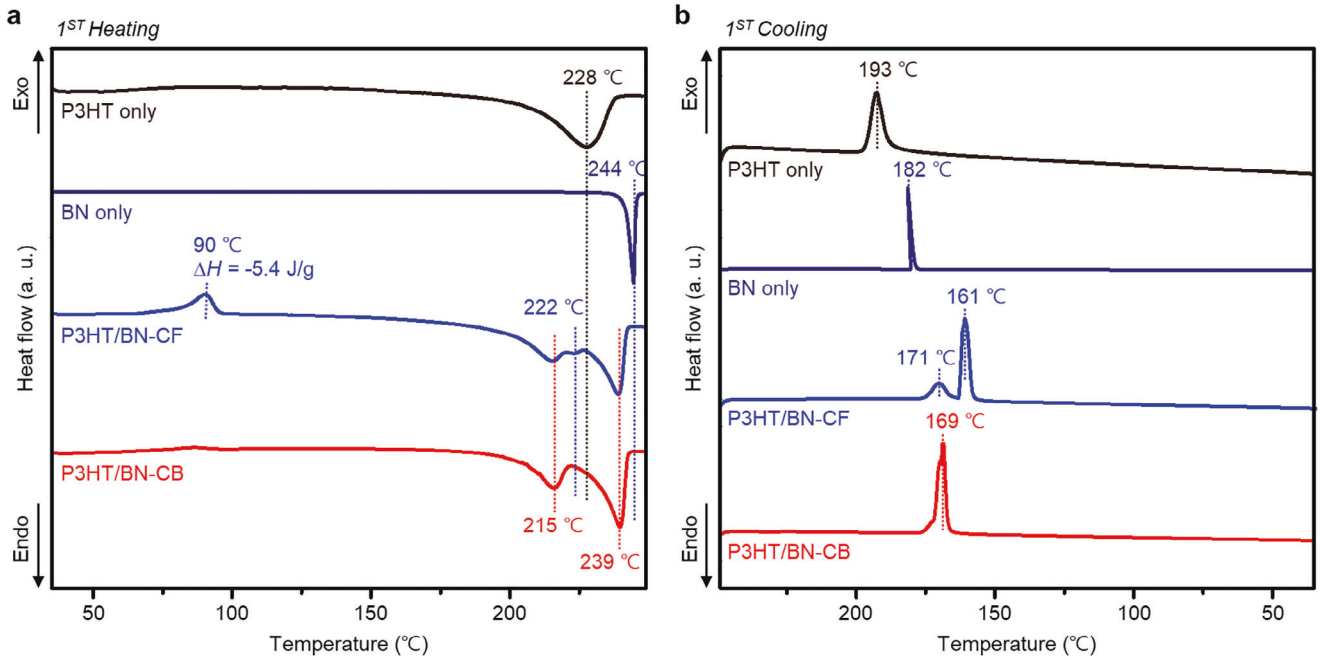

Figure 5. a–b) Differential scanning calorimetry first heating scan curves (a) and first cooling scan curves (b) for the P3HT (black), BN (dark blue), P3HT/BN-CF (blue), and P3HT/BN-CB (red) hybrids.

the CB solution, as shown in Figure 6d,g. This result indicates that P3HT molecules are preferentially stacked with an edge-on orientation in the P3HT/BN-CB hybrid film. When comparing the *d*-spacing of the P3HT crystalline structure in the hybrid film with that in the P3HT film, simultaneous increases in the (100) interlamellar distance and (010) π–π stacking distances of P3HT are observed (Figure 6j,l). Based on the comprehensive considerations for the formation of P3HT/BN co-crystals discussed above, BN molecules are inserted and co-crystallized within the lamellar stacking of P3HT, as shown in Figure 6m. The formation of such edge-on lamellar stacking of P3HT with inserted BN molecules was verified again in P3HT/BN hybrid films, which were prepared using another aromatic solvent of toluene, referred to as P3HT/BN-toluene. As shown in Figure 6e, the pristine P3HT film prepared from toluene exhibits (100) and (010) diffraction arcs, indicating the coexistence of edge-on- and face-on-oriented P3HT stacking. Notably, the P3HT/BN-toluene film exhibited significantly suppressed (010) intensity and much narrower (100) diffractions in q_z. This result demonstrates that hybridization with BN in an aromatic solvent promotes the edge-on lamellar stacking of P3HT, leading to a spherulitic co-crystal structure in the P3HT/BN-toluene hybrid film, as shown in Figure 2e. Based on this, we can conclude that the P3HT/BN hybrid film exhibiting transferred chiroptical transitions prepared using an aromatic organic solvent, forms spherulite crystals comprising co-crystallized lamellar with edge-on stacking of P3HT with inserted BN molecules.

To understand the photophysical molecular interaction between P3HT and BN molecules, photoluminescence-excitation (PLE) analysis of the hybrid solutions using CF and CB solvents is performed, as shown in **Figure 7**. For the PLE measurements, the weight concentration of P3HT (1.4×10^{-3} wt.%) and BN (0.7×10^{-3} wt.%) in each solution was the same, even in their mixed solution (2.1×10^{-3} wt.%). As shown in Figure 7b,e, the strong PL emission of BN at 400 nm was significantly quenched after mixing with P3HT in the solvent medium. This finding indicates that intermolecular fluorescent resonance energy transfer can occur from BN to P3HT in the solution state because the PL spectra of BN can overlap with the absorption spectra of P3HT.[74] To understand the molecular aggregate state, the emission spectra corresponding to the P3HT extracted from PLE analysis are shown in Figure 7g,h. When P3HT and BN are mixed in CF, the PL intensity of P3HT at an excitation wavelength of λ_{ex} = 525 nm significantly decreases to ≈19% of that observed in the P3HT-only solution (see Figure 7g). This PL decrease is attributed to the self-quenching effect caused by the enhanced aggregation of adjacent P3HT molecules after the addition of BN to the CF solution (Figure 7j).[75] In contrast, the P3HT emission in the CB increased by ≈31% after the addition of BN to the P3HT-only solution, as shown in Figure 7h. This finding suggests that the π–π interactions of aromatic CB molecules with P3HT hinder the formation of P3HT aggregates, even after the addition of BN in the solution, resulting in a molecularly well-mixed hybrid state of P3HT and BN (Figure 7k).[76] In this state, the amine (-NH_2) groups in BN can also affect the molecular interactions with P3HT. When the PL analysis is conducted for the CB solution with various binaphthyl derivatives containing different functional groups, such as hydroxyl (-OH), bromide (-Br), and methyl (-CH_3), significant quenching of P3HT emission is observed, similar to the P3HT/BN in the CF solution (Figure S12a,b, Supporting Information). The hybrid film based on these BN derivatives does not exhibit transferred chiroptical activity at the P3HT transitions (Figure S12c–e, Supporting Information). It is worth mentioning that the N–H···S

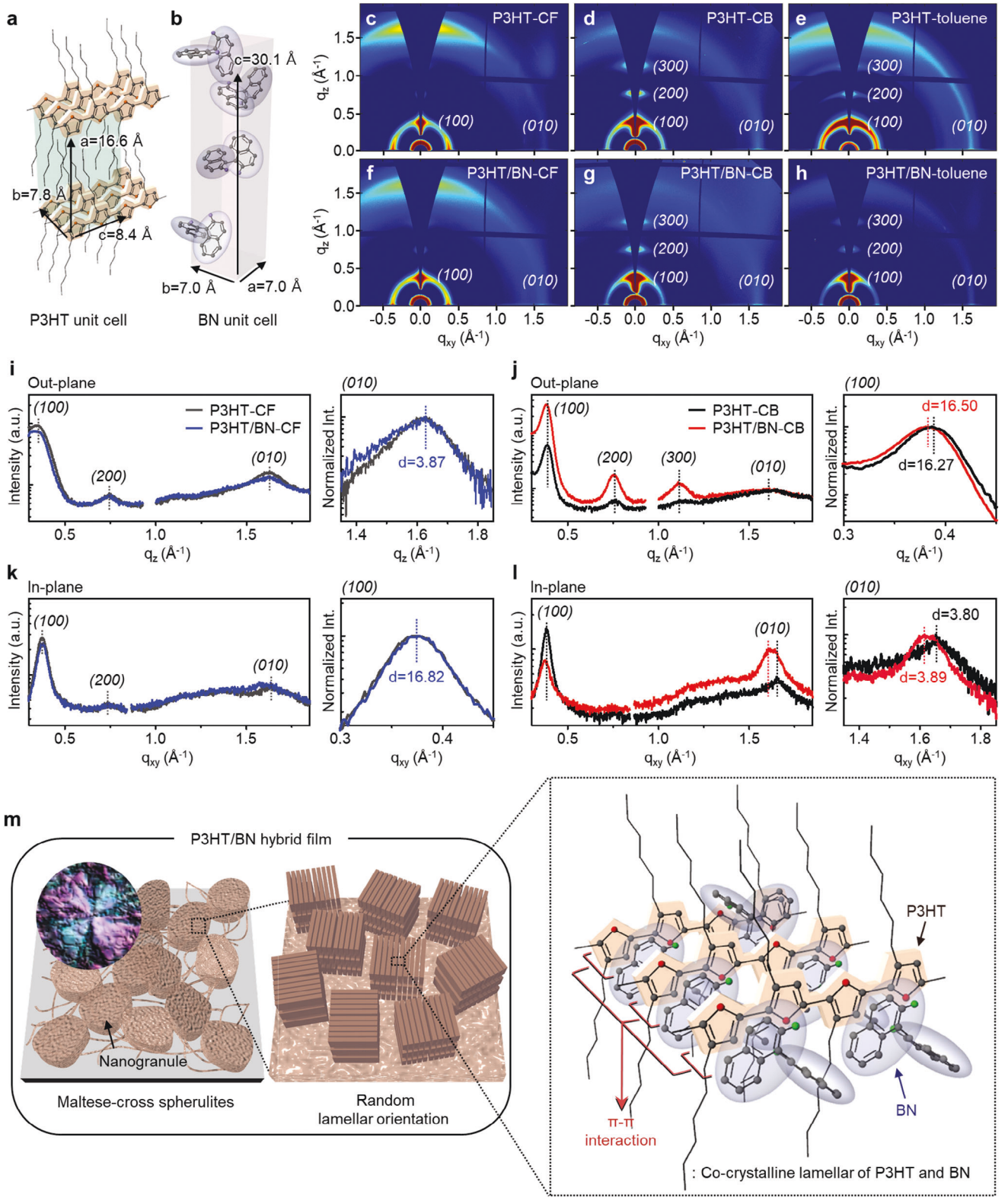

Figure 6. a–b) Unit cell of P3HT (a) and BN (b). c–h) 2D grazing-incidence X-ray diffraction (GIXD) images of the P3HT-CF (c), P3HT-CB (d), P3HT-toluene (e), P3HT/BN-CF (f), P3HT/BN-CB (g), and P3HT/BN-toluene (h). (i–j) Out-of-plane GIXD of pristine P3HT and P3HT/BN hybrid films using CF (i) and CB (j). (k–l) In-plane GIXD of pristine P3HT and P3HT/BN hybrid films using CF (k) and CB (l). (m) Schematic illustration for the spherulites of the P3HT/BN hybrid films, comprising co-crystalline lamellar of P3HT and BN.

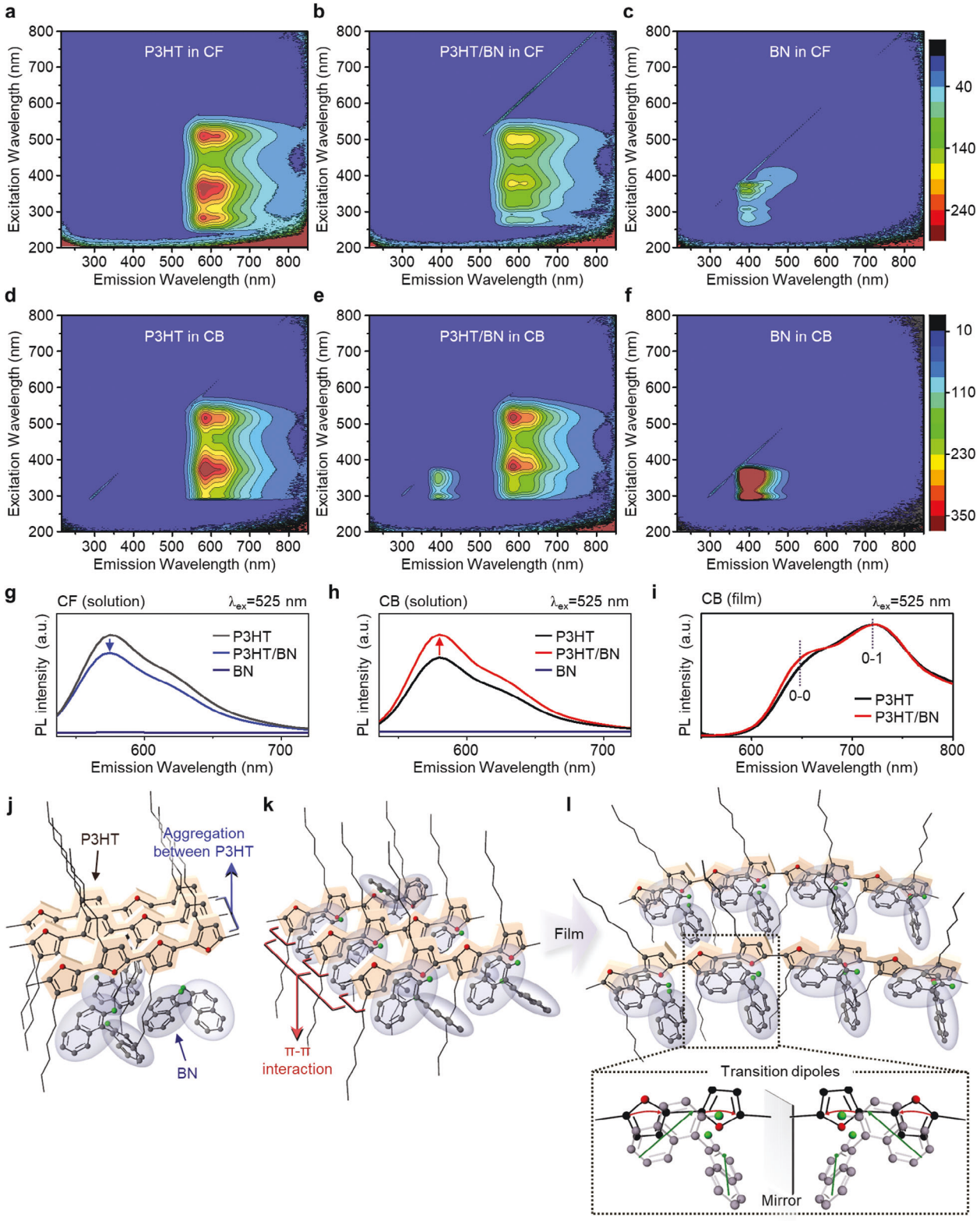

Figure 7. a–f) Photoluminescence-excitation (PLE) map of P3HT-only (a,d), P3HT/BN mixture (b,e), and BN-only (c,f) solutions in CF (top) and CB (bottom). All solutions were measured at the same concentration. g–h) PL spectra of the P3HT, P3HT/BN, and BN dissolved in CF (g) and CB (h) solution extracted from PLE analysis in Figure 7a–f. Laser pulses with a wavelength of 525 nm are used for photoexcitation. i) PL spectra of the pristine P3HT and P3HT/BN hybrid film. Laser pulses with a wavelength of 525 nm are used for photoexcitation. j–k) Schematic showing the aggregation of adjacent P3HT molecules in the CF solution (j) and the cofacial π–π interactions between P3HT and BN in the CB solution (k). l) Schematic showing the in-plane bending of the conjugated backbone during film formation.

hydrogen bonding interaction between the amine group of BN and the thiophene units of the P3HT backbone is possible, unlike the other derivatives.[77] The bathochromic shift of N–H stretches in BN, observed at 3476 and 3383 cm^{-1} in the FT-IR spectrum after mixing with P3HT, supports the presence of this interaction[78] (Figure S13, Supporting Information). Therefore, these results suggested that using an aromatic solvent resulted in the molecularly well-mixed P3HT and BN hybrid state capable of intermolecular π–π and hydrogen bonding interactions. Considering that aromatic organic solvents typically induce solvophobic interactions with the alkyl sidechains of π-CP and promote the self-assembled ordered structure,[9,79] it can be reasonably inferred that these solvents facilitate the formation of the co-crystalline lamellar structure of P3HT and BN during the solidification process of this hybrid solution.

To further investigate the effect of BN on the transferred chiroptical activity of the P3HT/BN-toluene hybrid film, we examined the morphologies and optical properties of the hybrid film after selectively dissolving BN by immersing it in dimethylsulfoxide (DMSO), a nonsolvent for P3HT. As shown in Figure S14 (Supporting Information), the selective dissolution of BN in the film is confirmed by the disappearance of its characteristic absorption peak. Interestingly, after selectively removing BN, the Maltese-cross spherulite structure in the P3HT/BN-CB hybrid film remained intact; however, the transferred CD response decreased significantly by ≈10-fold. This indicates that the transferred chiroptical transitions in the P3HT of the hybrid films are significantly influenced by the co-crystallized BN molecules.

Regarding the origin of chiroptical activity in π-CP/*chiral*-SM hybrid films, previous reports suggest considering helical conformation and twisted cylinder blue-phase.[26,30] In these cases, the collapse of lamellar molecular stacking and the development of long fibril structures were observed after the addition of a chiral inducer to the conjugated polymer, as evidenced by GIXD and AFM analyses. However, the demonstrated chiroptical P3HT/BN-CB film did not exhibit such fibrillar structures (Figure 4b); instead, the lamellar crystallization of P3HT was enhanced, as shown in Figure 6. Therefore, different mechanisms for the induction of chiroptical activity in the P3HT/BN-CB hybrid film need to be suggested.

Based on the Frenkel exciton model developed by Spano,[80] different coupling types (H- and J-aggregate) can be typically identified by intensity differences of PL in 0-0 ($I_{0\text{-}0}$) and 0–1 ($I_{0\text{-}1}$) vibronic transitions. H-type aggregate signatures, characterized by $I_{0-0}/I_{0-1} < 1$, result from dominant interchain coupling and a high degree of interchain order, whereas J-type aggregates, indicated by $I_{0\text{-}0}/I_{0\text{-}1} \geq 1$, arise from dominant intrachain coupling.[81–83] Previous literature has shown that the J-type coupling in P3HT crystalline structures is enhanced as the molecular weight of P3HT increases, because the folded chains in the lamellar crystallite increase, evidenced by the increase in I_{0-0}/I_{0-1} ratios.[83,84] Based on our PL spectrum shown in Figure 7i, the pristine P3HT film exhibited the PL intensity with $I_{0-0}/I_{0-1} < 1$, indicating that the H-type interchain exciton coupling is dominant. In comparison, the PL spectrum of the chiroptical P3HT/BN-CB film exhibited an increased $I_{0\text{-}0}$ relative to the $I_{0\text{-}1}$. This can be strong evidence that the J-type intramolecular coupling in P3HT increased after forming a co-crystalline lamellar structure with BN.[81,82] Additionally, the significant changes in CD response of BN and PL spectrum after hybridization in CB solvent, as shown in Figure 1c and Figure 7e, already supported the presence of the transition dipole couplings between BN and P3HT. Combined with PL evidence, this suggests that the presence of BN molecules inside the P3HT lamellar stacking induces asymmetrically misaligned transition dipoles in the P3HT chain by intermolecular orbital coupling, resulting in the transferred chiroptical activity in the P3HT (Figure 7l).

Finally, to verify the feasibility of the π-CP/*chiral*-SM hybrid films as chiroptical active layers for optoelectronic devices, photodiodes were fabricated. The device structure and energy band alignment are shown in **Figure 8a**.[47,85] SnO_2 was used as an electron-transport/hole-blocking layer to enhance the collection of photogenerated electrons. P3HT/BN-toluene film was then spin-cast on top of the SnO_2-coated indium tin oxide (ITO)/glass. To evaluate the CPL-sensing capability of the photodiode, the CPL with a 488 nm wavelength was illuminated from the bottom of the device (P_{IN} = 14.9 mW cm^{-2}). Figure 8b,c show that the photodiode based on the P3HT/BN hybrid film can distinguish the polarization direction of the CPL, where the (*R*)-P3HT/BN-based photodiode exhibits a higher photocurrent when exposed to right circularly polarized light (RCP), whereas the (*S*)-P3HT/BN film exhibits the opposite response. The dissymmetry factor for photocurrent (g_{ph}) was calculated to be 0.2, which was comparable to the previously reported organic chiroptical photodetectors.[8,11,47,86–88] In addition, a chiroptically responsive integrated photodiode array was demonstrated by simple printing of P3HT/BN hybrids (Figure 8d). Figure 8e shows a cross-polarized OM image of the device with a printed micropattern array of P3HT/BN on 3 × 8 a silicon-PN photodiode array. The device utilizes the P3HT/BN hybrid film as a chiroptical filter, enabling differential CPL absorption according to the chirality of BN, resulting in the generation of distinct photocurrents in the underlying PN diode. Figure 8f,g exhibits the real-time photocurrent changes recorded under repetitive optical on/off switch with a change in the polarization direction of the incident CPL (P_{IN} = 0.32 mW cm^{-2}). A PN diode with (*R*)-P3HT/BN exhibited a higher photocurrent for the CPL with left circularly polarized light (LCP) than that under RCP illumination. This demonstration underscores the potential of π-CP/*chiral*-SM hybrid films for advancing chiroptically responsive optoelectronic devices, offering promising avenues for future applications in chiral photonics and beyond.

3. Conclusion

In summary, we demonstrate that the choice of aromatic solvent is critical for the transfer of chiroptical activity to π-CPs in their hybrids with chiral binaphthyl diamine additives. Chiroptical transitions in the light absorption range of 350–850 nm were generated from various π-CPs, including polythiophene and diketopyrrolopyrrole-based D-A-type polymers, by simply blending them with chiral BN molecules, especially using aromatic solvents. The π-CP/*chiral*-BN hybrid films with transferred chiroptical responses exhibited characteristic Maltese cross birefringence, indicating the formation of polymer spherulites with lamellar stacking. The versatility of chirality transfer in π-CP/*chiral*-BN hybrid films for various aromatic solvents was verified, enabling the printing of chiroptical micropattern arrays with

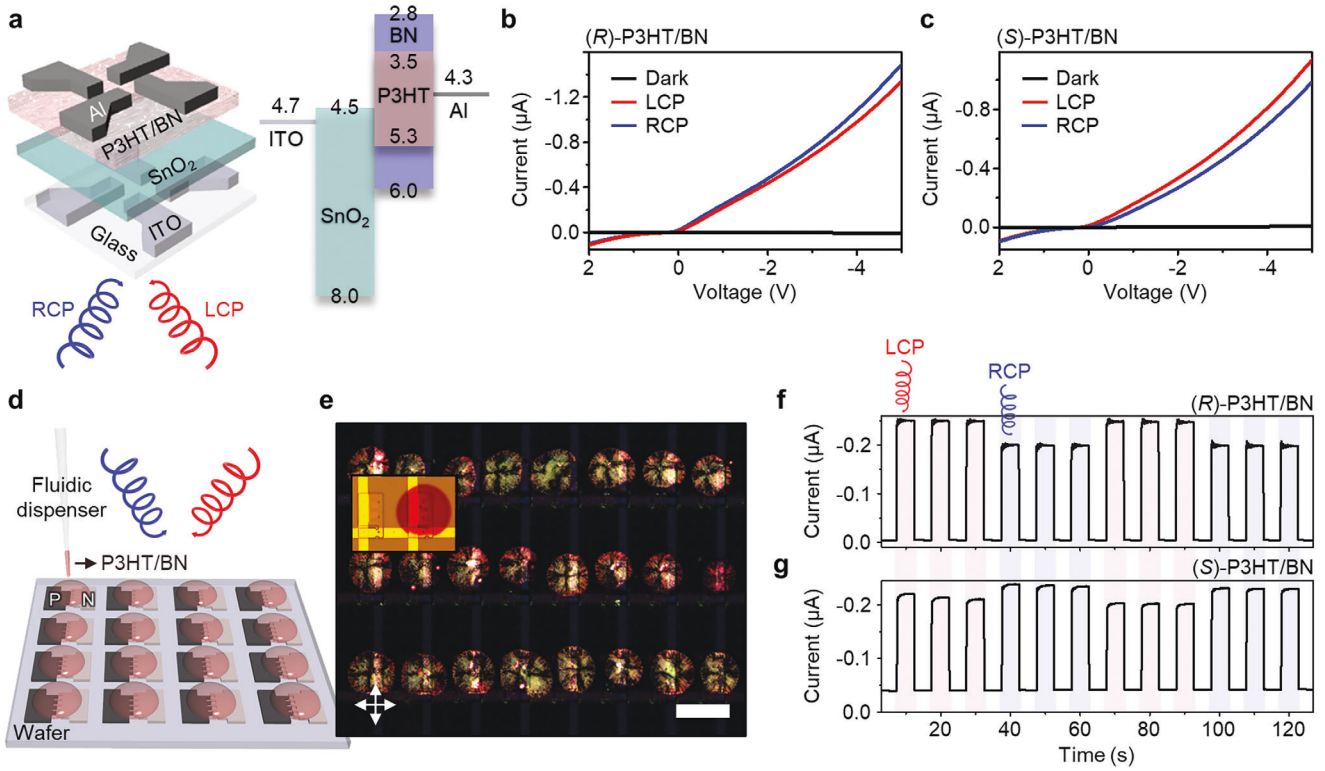

Figure 8. a) Schematic showing the photodiode based on P3HT/BN, where the channel area is 0.4 cm^2. The flat energy-band diagram formed between indium tin oxide (ITO), SnO_2, P3HT/BN, and Al. b–c) I-V curve of photodiode based on (*R*)-P3HT/BN (b) and (*S*)-P3HT/BN (c) upon irradiation with left circularly polarized light (LCP) (red line) and right circularly polarized light (RCP) (blue line) light (λ = 488 nm, P_{IN} = 14.9 mW cm^{-2}). d) Schematic showing the PN diode based on P3HT/BN, where the channel area is 0.0034 cm^2. e) POM image of circular micropattern on the PN diode. Inset shows OM image of the PN diode and PN diode with P3HT/BN (polarization angle = 90°, scale bar = 100 μm). f, g) Time-dependent photocurrent signals of PN diode based on (*R*)-P3HT/BN (f) and (*S*)-P3HT/BN (g) upon irradiation with LCP and RCP light (λ = 488 nm, P_{IN} = 0.32 mW cm^{-2}) according to real-time optical on/off switch with repeated conversion of the CPL polarization direction. Time intervals are constant, with light on for 5 s and off for 5 s, and the applied voltage was −1 V.

a single spherulite structure. Investigations into the morphologies, phase behaviors, and crystalline structure of P3HT/BN hybrid films revealed that the chiral BN molecules were co-crystallized into edge-on lamellar stacking of the P3HT chains in the nanogranules when only CB aromatic solvent was used in the film-forming process. In-depth studies on the photophysical properties between chiral BN molecules and P3HT chains suggested that the coexistence of chiral BN molecules was important for chirality induction in π-CPs, where electronic coupling induced misaligned transition dipoles in the P3HT intrachain, which was attributed to the transferred chiroptical transitions in π-CPs. As a proof-of-concept, a photodiode based on a chiroptical P3HT/BN hybrid film exhibited distinguishable photoresponse to chiral light with different circular polarization directions. This study provides a versatile strategy for fabricating chiroptical semiconductor thin films using various π-CPs with a variety of functionalities, which is expected to encourage further studies and contribute to extending the applications of chiral optoelectronics.

4. Experimental Section

Materials: P3HT (weight-average molecular weight = 50–70 kDa), (*R*)-BN, and (*S*)-BN were used as received from Rieke Metals. PTB7 (weight-average molecular weight = 50–90 kDa) and PFO were purchased from Solaris Chem and H.W. Sands Corp., respectively. In addition, P(DPPTBT) was synthesized according to previously reported methods.[4] Several solvents, including CF, CB, toluene, xylene, DCB, TCB, tetralin, and DMSO were purchased from Sigma-Aldrich and were used without further purification.

Sample Preparation: The polymers (P3HT, PTB7, PFO, or P(DPPTBT)) and chiral materials ((*R*)-BN or (*S*)-BN) were dissolved in organic solvents, in which the ratio of the polymer components was 66.6% while maintaining the concentration at 3.3 wt.%. The blend solution was then stirred overnight at room temperature. To control the thickness of the film before coating, only the solution using chloroform was diluted to a concentration of 1.1 wt.%. Quartz was used as the substrate and was cleaned with acetone and isopropyl alcohol before coating. The blend solution was annealed at 45 °C for 10 min and then spin-coated to fabricate the hybrid film with a thickness of ≈200 nm.

Printing of the Micro-Patterns: The blend solution dissolved in TCB was printed into circular micro-patterns using a picoliter fluidic dispenser (SonoPlot Inc.) with 50 or 10 μm orifice glass tips on the substrate under ambient room temperature conditions. The blend solutions were ejected and drawn from the glass tip by controlling the piezoelectrics.

Fabrication of Photodiode: ITO-coated glass substrates were cleaned with DI water, acetone, and isopropyl. After the substrate was treated using a UV–ozone cleaner (AH1700, Ahtech Ltd.) for 10 min, SnO_2 thin films were spin-coated at 2000 rpm for 30 s and then thermal-treated for 5 min at 120 °C. Then, 200 nm-thick P3HT/BN hybrid film was spin-coated (4000 rpm for 50 s) from the hybrid solution with toluene solvent. The silicon-PN photodiode array was fabricated according to previously reported methods.[89] The blend solution dissolved in TCB was printed into

circular micro-patterns using a picoliter fluidic dispenser, as explained previously.

Characterization: The optical absorption and the CD spectra of solutions and films were acquired using a UV-Vis-NIR spectrometer (Lambda 750, Perkin Elmer) and a CD spectrometer (J-1500, JASCO), respectively. The thicknesses of the films were determined using a surface profiler (AlphaStep As-IQ, KLA-Tencor). The thermal transition temperature of the films was determined using a differential scanning calorimeter (DSC400, Perkin Elmer) at a heating rate of 5 °C min^{-1} under a nitrogen atmosphere. The morphologies of thin films were studied using a polarized optical microscope (LV150N, Nikon) and AFM (XE-100, Park systems) measurements. Vibrational imaging with s-SNOM was conducted utilizing an atomic force microscope/near-field platform and infrared quantum cascade laser (QCL, MIRcat-QT-Z-2400 of Daylight Solutions) as an excitation source, as described in our recent publications.[90,91] The QCL produced linearly polarized IR radiation with a tunable frequency and ≈0.1 cm^{-1} resolution. The AFM operated in the noncontact tapping mode, utilizing a metal-coated probe (Arrow NCPt) with a resonance frequency of ≈270 kHz. The vertically polarized output of the QCL was focused at the tip-sample junction using a parabolic mirror (NA of ≈0.46) at a 30° angle of incidence with respect to the sample plane. Laser power was maintained at 3 mW across all QCL frequencies through the use of dual polarizers. Photons scattered from the nanoscale region of tip-sample near-field interaction were detected using HgCdTe photodiodes cooled with liquid nitrogen. The far-field background signal was removed using pseudoheterodyne interferometric detection and signal demodulation at a frequency of 3 Ω. Photoluminescence-excitation (PLE) map and photoluminescence (PL) spectra were measured using a PL spectrometer (FP-8500, JASCO). 2D-GIXD patterns were performed at the 3C-SAXS beamline of the Pohang Accelerator Laboratory in Korea. The wavelength and grazing angle of the incident X-ray beam were 1.1975 Å and 0.12°, respectively.

Supporting Information

Supporting Information is available from the Wiley Online Library or from the author.

Acknowledgements

This study was supported by the Air Force Office of Scientific Research under award number FA2386-24-1-4030 and FA2386-21-1-4102. This study was also supported by the National Research Foundation of Korea (NRF) (RS-2024-00452255), Future Resource Research Program of the Korea Institute of Science and Technology (KIST) (2E33191), and US National Science Foundation (Award No. 2154617).

Conflict of Interest

The authors declare no conflict of interest.

Data Availability Statement

The data that support the findings of this study are available from the corresponding author upon reasonable request.

Keywords

binaphthyl, chiral inducer, chirality transfer, chiroptical semiconductor, conjugated polymer blend

Received: June 8, 2024
Revised: July 17, 2024
Published online:

[1] J. Crassous, M. J. Fuchter, D. E. Freedman, N. A. Kotov, J. Moon, M. C. Beard, S. Feldmann, *Nat. Rev. Mater.* **2023**, *8*, 365.
[2] J. R. Brandt, F. Salerno, M. J. Fuchter, *Nat. Rev.Chem.* **2017**, *1*, 0045.
[3] J. F. Sherson, H. Krauter, R. K. Olsson, B. Julsgaard, K. Hammerer, I. Cirac, E. S. Polzik, *Nature* **2006**, *443*, 557.
[4] H. Han, Y. J. Lee, J. Kyhm, J. S. Jeong, J. H. Han, M. K. Yang, K. M. Lee, Y. Choi, T. H. Yoon, H. Ju, *Adv. Func. Mater.* **2020**, *30*, 2006236.
[5] M. Khorasaninejad, W. Chen, A. Zhu, J. Oh, R. Devlin, D. Rousso, F. Capasso, *Nano Lett.* **2016**, *16*, 4595.
[6] W. H. Brooks, W. C. Guida, K. G. Daniel, *Curr. Top. Med. Chem.* **2011**, *11*, 760.
[7] S. D. Namgung, R. M. Kim, Y.-C. Lim, J. W. Lee, N. H. Cho, H. Kim, J.-S. Huh, H. Rhee, S. Nah, M.-K. Song, *Nat. Comm.* **2022**, *13*, 5081.
[8] L. Zhang, I. Song, J. Ahn, M. Han, M. Linares, M. Surin, H.-J. Zhang, J. H. Oh, J. Lin, *Nat. Comm.* **2021**, *12*, 142.
[9] H. Lee, J. H. Hwang, S. H. Song, H. Han, S. J. Han, B. L. Suh, K. Hur, J. Kyhm, J. Ahn, J. H. Cho, *Adv. Sci.* **2023**, *10*, 2304039.
[10] M. Schulz, F. Balzer, D. Scheunemann, O. Arteaga, A. Lützen, S. C. Meskers, M. Schiek, *Adv. Funct. Mater.* **2019**, *29*, 1900684.
[11] J. Gilot, R. Abbel, G. Lakhwani, E. Meijer, A. P. Schenning, S. C. Meskers, *Adv. Mater.* **2010**, *22*, E131.
[12] H. Han, J. H. Choi, J. Ahn, H. Lee, C. Choi, W. Jung, J. Yeom, D. K. Hwang, B. J. Sung, J. A. Lim, *ACS Appl. Mater. Interfaces* **2023**, *15*, 57447.
[13] J. Wang, C. Fang, J. Ma, S. Wang, L. Jin, W. Li, D. Li, *ACS Nano* **2019**, *13*, 9473.
[14] H. Y. Hou, S. Tian, H. R. Ge, J. D. Chen, Y. Q. Li, J. X. Tang, *Adv. Funct. Mater.* **2022**, *32*, 2209324.
[15] J. Schmidt, A. Guggenmos, M. Hofstetter, S. H. Chew, U. Kleineberg, *Opt. Express* **2015**, *23*, 33564.
[16] F. J. Rodríguez-Fortuño, I. Barber-Sanz, D. Puerto, A. Griol, A. Martínez, *ACS Photonics* **2014**, *1*, 762.
[17] C. Kulkarni, M. H. van Son, D. Di Nuzzo, S. C. Meskers, A. R. Palmans, E. Meijer, *Chem. Mater.* **2019**, *31*, 6633.
[18] G. Albano, G. Pescitelli, L. Di Bari, *Chem. Rev.* **2020**, *120*, 10145.
[19] S. Huang, H. Yu, Q. Li, *Adv. Sci.* **2021**, *8*, 2002132.
[20] Y. Xue, C. Zhang, T. Lv, L. Qiu, F. Wang, *Angew. Chem., Int. Ed.* **2023**, *62*, 202300972.
[21] K. Dhbaibi, C. Shen, M. Jean, N. Vanthuyne, T. Roisnel, M. Górecki, B. Jamoussi, L. Favereau, J. Crassous, *Front. Chem.* **2020**, *8*, 237.
[22] T. Miao, X. Cheng, H. Ma, Z. He, Z. Zhang, N. Zhou, W. Zhang, X. Zhu, *Angew.Chem* **2021**, *133*, 18714.
[23] R. Hu, X. Lu, X. Hao, W. Qin, *Adv. Mater.* **2023**, *35*, 2211935.
[24] H. Kim, D. Lee, S. Lee, N. Suzuki, M. Fujiki, C. L. Lee, G. Kwak, *Macromol. Rapid Commun.* **2013**, *34*, 1471.
[25] Y. Zhang, J. Deng, K. Pan, *Macromolecules* **2018**, *51*, 8878.
[26] I. Song, J. Ahn, H. Ahn, S. H. Lee, J. Mei, N. A. Kotov, J. H. Oh, *Nature* **2023**, *617*, 92.
[27] J. Wade, J. R. Brandt, D. Reger, F. Zinna, K. Y. Amsharov, N. Jux, D. L. Andrews, M. J. Fuchter, *Angew. Chem., Int. Ed.* **2021**, *60*, 222.
[28] Y. Zhang, H. Li, Z. Geng, W.-H. Zheng, Y. Quan, Y. Cheng, *ACS Nano* **2022**, *16*, 3173.
[29] D. M. Lee, J. W. Song, Y. J. Lee, C. J. Yu, J. H. Kim, *Adv. Mater.* **2017**, *29*, 1700907.
[30] J. Wade, J. N. Hilfiker, J. R. Brandt, L. Liirò-Peluso, L. Wan, X. Shi, F. Salerno, S. T. Ryan, S. Schöche, O. Arteaga, *Nat. comm.* **2020**, *11*, 6137.
[31] C. Dai, Y. Wang, Y. Quan, Q. Chen, Y. Cheng, C. Zhu, *J. Polym. Sci. A Polym. Chem.* **2014**, *52*, 3080.
[32] L. Liu, Z. Wei, S. C. Meskers, *Adv. Mater.* **2023**, *35*, 2209730.
[33] L. Liu, Y. Yang, L. Zhu, J. Zhang, K. Chen, Z. Wei, *Small* **2022**, *18*, 2202941.

[34] M. D. Ward, J. Wade, X. Shi, J. Nelson, A. J. Campbell, M. J. Fuchter, *Adv. Opt. Mater.* **2022**, *10*, 2101044.
[35] Y. Zhang, D. Li, Q. Li, Y. Quan, Y. Cheng, *Adv. Funct. Mater.* **2023**, *33*, 2309133.
[36] L. Wan, J. Wade, X. Wang, A. J. Campbell, M. J. Fuchter, *J. Mater. Chem. C.* **2022**, *10*, 5168.
[37] L. Wan, J. Wade, F. Salerno, O. Arteaga, B. Laidlaw, X. Wang, T. Penfold, M. J. Fuchter, A. J. Campbell, *ACS Nano* **2019**, *13*, 8099.
[38] Z. Chen, C. Zhong, J. Han, J. Miao, Y. Qi, Y. Zou, G. Xie, S. Gong, C. Yang, *Adv. Mater.* **2022**, *34*, 2109147.
[39] P. Duan, H. Cao, L. Zhang, M. Liu, *Soft Matter* **2014**, *10*, 5428.
[40] Y. Kira, Y. Okazaki, T. Sawada, M. Takafuji, H. Ihara, *Amino Acids* **2010**, *39*, 587.
[41] X. Zhu, P. Duan, L. Zhang, M. Liu, *Chem.-Eur. J.* **2011**, *17*, 3429.
[42] Y. Li, T. Wang, M. Liu, *Soft Matter* **2007**, *3*, 1312.
[43] D. Yang, P. Duan, L. Zhang, M. Liu, *Nat. Comm.* **2017**, *8*, 15727.
[44] K. Watanabe, I. Osaka, S. Yorozuya, K. Akagi, *Chem. Mater.* **2012**, *24*, 1011.
[45] P. Wang, I. Jeon, Z. Lin, M. D. Peeks, S. Savagatrup, S. E. Kooi, T. Van Voorhis, T. M. Swager, *J. Am. Chem. Soc.* **2018**, *140*, 6501.
[46] B. E. Risteen, A. Blake, M. A. McBride, C. Rosu, J. O. Park, M. Srinivasarao, P. S. Russo, E. Reichmanis, *Biomacromolecules* **2017**, *18*, 1556.
[47] N. Y. Kim, J. Kyhm, H. Han, S. J. Kim, J. Ahn, D. K. Hwang, H. W. Jang, B. K. Ju, J. A. Lim, *Adv. Funct. Mater.* **2019**, *29*, 1808668.
[48] J. Liu, Z. P. Song, L. Y. Sun, B. X. Li, Y. Q. Lu, Q. Li, *Resp. Mater.* **2023**, *1*, 20230005.
[49] H. Wang, Y. Tang, H. K. Bisoyi, Q. Li, *Angew. Chem.* **2023**, *135*, 202216600.
[50] X. Zhang, Y. Xu, C. Valenzuela, X. Zhang, L. Wang, W. Feng, Q. Li, *Light Sci. Appl.* **2022**, *11*, 223.
[51] A. Shockravi, A. Javadi, E. Abouzari-Lotf, *RSC Adv.* **2013**, *3*, 6717.
[52] Y. Zhang, H. Li, Z. Geng, W. Zheng, Y. Quan, Y. Cheng, *Nat. Comm.* **2022**, *13*, 4905.
[53] Z. Geng, Y. Zhang, Y. Zhang, Y. Quan, Y. Cheng, *Angew. Chem.* **2022**, *134*, 202202718.
[54] M. Schulz, J. Zablocki, O. S. Abdullaeva, S. Brück, F. Balzer, A. Lützen, O. Arteaga, M. Schiek, *Nat. Comm.* **2018**, *9*, 2413.
[55] M. R. Craig, P. Jonkheijm, S. C. Meskers, A. P. Schenning, E. Meijer, *Adv. Mater.* **2003**, *15*, 1435.
[56] B. A. San Jose, S. Matsushita, K. Akagi, *J. Am. Chem. Soc.* **2012**, *134*, 19795.
[57] Z. Geng, Y. Zhang, Y. Zhang, Y. Li, Y. Quan, Y. Cheng, *J. Mater. Chem. C* **2021**, *9*, 12141.
[58] H. Zhang, X. Zheng, R. T. Kwok, J. Wang, N. L. Leung, L. Shi, J. Z. Sun, Z. Tang, J. W. Lam, A. Qin, *Nat. Comm.* **2018**, *9*, 4961.
[59] L. Di Bari, G. Pescitelli, P. Salvadori, *J. Am. Chem. Soc.* **1999**, *121*, 7998.
[60] S. F. Mason, R. H. Seal, D. Roberts, *Tetrahedron* **1974**, *30*, 1671.
[61] B. Crist, J. M. Schultz, *Prog. Polym. Sci.* **2016**, *56*, 1.
[62] Y. Li, Z. Wang, T. He, *Crystals* **2017**, *7*, 115.
[63] C. Müller, M. Aghamohammadi, S. Himmelberger, P. Sonar, M. Garriga, A. Salleo, M. Campoy-Quiles, *Adv. Funct. Mater.* **2013**, *23*, 2368.
[64] Y. Li, H. Huang, Z. Wang, T. He, *Macromolecules* **2014**, *47*, 1783.
[65] Z. Wang, G. C. Alfonso, Z. Hu, J. Zhang, T. He, *Macromolecules* **2008**, *41*, 7584.
[66] K. Whitehead, M. Grell, D. Bradley, M. Jandke, P. Strohriegl, *Appl. Phys. Lett.* **2000**, *76*, 2946.
[67] Y. Liang, Z. Xu, J. Xia, S.-T. Tsai, Y. Wu, G. Li, C. Ray, L. Yu, *Adv. Mater.* **2010**, *22*, E135.
[68] P. Sonar, S. P. Singh, Y. Li, M. S. Soh, A. Dodabalapur, *Adv. Mater.* **2010**, *22*, 5409.
[69] N. E. Persson, P.-H. Chu, M. McBride, M. Grover, E. Reichmanis, *Acc.Chem. Res.* **2017**, *50*, 932.
[70] T. E. Tesema, R. McFarland-Porter, E. Zerai, J. Grey, T. G. Habteyes, *J. Phys. Chem. C.* **2022**, *126*, 7764.
[71] J. Xin, X. Meng, X. Xu, Q. Zhu, H. B. Naveed, W. Ma, *Matter* **2019**, *1*, 1316.
[72] D. H. Kim, J. T. Han, Y. D. Park, Y. Jang, J. H. Cho, M. Hwang, K. Cho, *Adv. Mater.* **2006**, *18*, 719.
[73] M. D. Jones, F. A. Almeida Paz, J. E. Davies, B. F. G. Johnson, *Acta Cryst.* **2003**, *59*, o910.
[74] X. Zhang, Z. Xu, Y. Zhang, Y. Quan, Y. Cheng, *ACS Appl. Mater. Interfaces* **2021**, *13*, 55420.
[75] K. M. Alam, J. C. Garcia, M. V. Kiriakou, N. Chaulagain, D. Vrushabendrakumar, E. D. Cranston, S. Gusarov, A. E. Kobryn, K. Shankar, *Nanotechnology* **2023**, *34*, 205703.
[76] G. E. Purdum, X. Chen, N. Telesz, S. M. Ryno, N. Sengar, T. Gessner, C. Risko, P. Clancy, R. T. Weitz, Y.-L. Loo, *Chem. Mater.* **2019**, *31*, 9691.
[77] M. R. Koebel, A. Cooper, G. Schmadeke, S. Jeon, M. Narayan, S. Sirimulla, *J. Chem. Inf. Model.* **2016**, *56*, 2298.
[78] M. F. Roberts, S. A. Jenekhe, *Macromolecules* **1991**, *24*, 3142.
[79] K. Watanabe, K. Suda, K. Akagi, *J. Mater. Chem. C.* **2013**, *1*, 2797.
[80] F. C. Spano, *Acc. Chem. Res.* **2010**, *43*, 429.
[81] L. Minion, J. Wade, J. M. Moreno-Naranjo, S. Ryan, G. Siligardi, M. J. Fuchter, *Chirality* **2023**, *35*, 817.
[82] N. J. Hestand, F. C. Spano, *J. Phys. Chem. B.* **2014**, *118*, 8352.
[83] M. Baghgar, J. A. Labastide, F. Bokel, R. C. Hayward, M. D. Barnes, *J. Phy. Chem. C.* **2014**, *118*, 2229.
[84] M. Baghgar, M. D. Barnes, *ACS Nano* **2015**, *9*, 7105.
[85] M. Meskini, S. Asgharizadeh, *Sci. Rep.* **2024**, *14*, 5723.
[86] L. Liu, Y. Yang, Y. Wang, M. A. Adil, Y. Zhao, J. Zhang, K. Chen, D. Deng, H. Zhang, K. Amin, *ACS Mater.Lett.* **2022**, *4*, 401.
[87] Z. Wang, M. Gao, X. Hao, W. Qin, *Appl. Phys. Lett.* **2020**, *116*, 053301.
[88] L. Wan, R. Zhang, E. Cho, H. Li, V. Coropceanu, J.-L. Brédas, F. Gao, *Nat. Photonics* **2023**, *17*, 649.
[89] M. Kim, S. Chang, M. Kim, J.-E. Yeo, M. S. Kim, G. J. Lee, D.-H. Kim, Y. M. Song, *Sci. Robot.* **2023**, *8*, eade4698.
[90] C.-F. Wang, B. Kafle, T. E. Tesema, H. Kookhaee, T. G. Habteyes, *J. Phys. Chem. C.* **2020**, *124*, 21018.
[91] W. M. Takele, T. G. Habteyes, *J. Phys. Chem. C.* **2024**, *128*, 2052.